Proceedings of the 5th International Symposium on Steel Science (ISSS 2017)
Nov. 13-16, 2017, Kyoto, Japan: The Iron and Steel Institute of Japan

Ferrite growth rate estimated from concentration profile measured using aberration corrected STEM-EELS

Takafumi Amino[1*], Genichi Shigesato[2], Takayuki Nozaki[3], Masafumi Azuma[4]

[1] Advanced Technology Research Laboratories, Nippon Steel & Sumitomo Metal Corporation, 1-8 Fuso-Cho, Amagasaki City, Hyogo 660-0891, Japan
[2] Steel Research Laboratories, Nippon Steel & Sumitomo Metal Corporation, 20-1 Shintomi, Futtsu City, Chiba. 293-8511, Japan
[3]Nagoya Works, Nippon Steel & Sumitomo Metal Corporation, 5-3, Tokaimachi, Tokai City, Aichi 476-8686, Japan
[4]Nagoya R&D Laboratory, Nippon Steel & Sumitomo Metal Corporation, 5-3, Tokaimachi, Tokai City, Aichi 476-8686, Japan

Abstract: Allotoriomorphic ferrite, which is the first to appear in the cooling of austenite, is required to precisely predict the growth behavior of the ferrite grains in order to control the fraction of the consituent. In the growth of the ferrite grains of Fe-C-X ternary alloy, the equilibrium state of the ferrite / austenite interface is different. Depending on whether the diffusion of X can follow the interfacial movement, the interface is in local-equilibrium or paraequilibrium, respectively. The growth rate of the ferrite grains is fast in the early stage and then decreases in velocity. Therefore, the equilibrium states of the interface transits. Solute drag by the interfacial segregation of alloying elements also affects the growth rate of ferrite grains. Experimental verification on balance of local equilibrium state and interfacial segregation during ferrite growth process is not sufficient. In this study, the growth behavior of the ferrite grains of ternary model alloys Fe-C-Mn in the isothermal holding was investigated using an optical microscope. Furthermore, the concentration profiles of Mn near the ferrite / martensite interfaces were measured by aberration corrected scanning transmission electron microscopy with electron energy loss spectroscopy, STEM-EELS. Using the solute drag theory, the growth rate of the ferrite grains was estimated. As a result, the growth behavior of the ferrite grains estimated by the STEM-EELS and solute drag theory was similar to the growth behavior estimated by the optical microscope observation.

1. INTRODUCTION

The mechanical properties of the multi-phase steel containing allotoriomorphic ferrite are related to the microstructure, which is formed by the phase transformation. Controlling the volume fraction of allotoriomorphic ferrite grains, which are the first to appear in the cooling of austenite, is important to control the other microstructures. The concentration of alloying elements of austenite during ferrite grain growth varies depending on the ferrite fraction, which affects the structure generated at a lower temperature. Therefore, properly understanding the ferrite transformation mechanism is important from the viewpoint of microstructural control.

In the growth of the ferrite grains of Fe-C-X ternary alloy, the equilibrium state of the ferrite / austenite interface is different. Where X represents a substitutional alloying element. Depending on whether the diffusion of X can follow the interfacial movement or not, the interface is in local-equilibrium [1], LE, or paraequilibrium [2], PE, respectively. The case of LE is further divided into two modes according to whether or not there is partitioning of X, partitioning local equilibrium (PLE) or negligible partitioning local equilibrium (NPLE) [1]. These interface conditions for ferrite transformation have been investigated by numerous studies [3]. Additionally, the transition of the equilibrium state from PE to NPLE was suggested in some studies [4-6].

Hillert [6] describes the transition behavior in detail. Firstly, the ferrite grain grows in PE. In this condition, neither local equilibrium of X nor partitioning of X occurs. Secondly, the transition from PE to NPLE occurs. The concentration of X at the contact point between the interface and austenite reaches LE. However, partitioning doesn't occur. Thirdly, the concentration of X at the contact point of the

* Corresponding author. E-mail: amino.b7x.takafumi@jp.nssmc.com, telephone: +81-6-6489-5736.

austenite side achieves NPLE. The concentration of X at the contact point with the austenite side has maximum concentration in the transition behavior. In this condition, partitioning has not started yet. Finally, the condition changes to PLE. In this condition, both partition and local equilibrium of X occur. The concentration of X at the contact point with the austenite side has decreased from NPLE.

It is expected that the velocity of the moving interface gradually decreases as the transition progresses. Thus, many investigations of ferrite transformation kinetics have been conducted based on the comparison between the ferrite growth rates obtained by calculations and observations [4-14]. As a result, fast growth of ferrite without partitioning and slow growth with partitioning of X have been established [7-9].

However, the behavior of ferrite growth cannot be explained only by the transition process described above. The transition behavior does not deal with the condition of the interface. The solute drag force caused by segregation of X to the interface should be estimated precisely in order to interprit experimental results of the ferrite growth rate [3,15-17]. The relationship between the transition behavior and solute drag effect on ferrite growth has not been made apparent.

One of the best solutions to this subject is to investigate the time variation of the concentration of X at the interface and the concentration profile near the interface with high accuracy and spatial resolution. Some attempts to measure the concentration of X at the interface have been reported [5, 17-19]. Guo et al. [19] measured the distribution of Mn at the interface in an Fe-C-Mn alloy using STEM-EDS and found the kinetic transition. They reported, in the first stage neither partitioning nor interface accumulation was detected, in the second stage no partitioning, but interfacial accumulation of Mn was recognized and in the third stage partitioning became apparent. Capdevila et al. [5] also found similar results using STEM-EELS. From the quantitative point of view, however, it is difficult from their results to identify whether the interfacial accumulation is the interfacial segregation or the spike of NPLE due to the insufficiency of spatial resolution. The spatial resolution of the previous studies seems to be several nm, whereas the width of the interface is considered to be less than 1 nm. Therefore, it is difficult to know the true concentration at the interface and estimate the solute drag effect quantitatively.

In order to measure the concentration of solute elements at the interface with an atomic resolution and estimate the true concentration profile, several factors affecting the resolution and accuracy, (i.e. the probe size, electron scattering in a specimen, the angle between the beam direction and the interface plane, etc.) should be considered carefully. One of the authors has developed a method to measure the concentration profile of boron segregated to austenite grain boundaries with high spatial resolution, using aberration corrected STEM-EELS [20].

In this study, the behavior of allotriomorphic ferrite formation during isothermal annealing at 973 K in Fe-0.12C-2.0Mn (mass %) is investigated. The kinetic transition is shown by measuring the ferrite thickening rate. Additionally, the time evolution of the Mn concentration profile at the interface is revealed by means of the measurement of the Mn concentration profile in the vicinity of the interface using aberration corrected STEM-EELS. The transition of kinetics and the interfacial condition of the isothermal transformation in the alloy are discussed. Furthermore, the solute drag effect on the ferrite growth is estimated by inserting the concentration of Mn segregated to the interface into the solute drag equation to describe a phase boundary [21, 22].

2. EXPERIMENTAL PROCEDURE

An ingot of Fe-0.12C-2.0Mn (mass %) was hot-rolled to 30 mm. The homogenization heat treatment was conducted at 1473 K for 48 hours in an Ar gas flow. The specimens of 10 mm x 80 mm x 1 mm were made by cutting from the center of the ingot. The specimens were austenitized at 1373 K for 60 s in an Ar atmosphere, cooled to 973 K using N_2 gas at 50 K/s, annealed at 973 K for 30, 300, 600, 3000, 10000, and 100000 s, and then quenched to room temperature using He gas. The microstructure etched with 3 % nital was observed by an optical microscope. The mean thickness of ferrite was measured from the optical microscope images. The thickness of ferrite was the average of the ten largest ferrite grains.

To compare with the result of the optical microscope observation, an isothermal section of Fe-C-Mn ternary phase diagram at 973 K with NPLE, PLE and PE region was calculated by Thermo Calc, version S with TCFE5 database. The width of ferrite grains assuming PE and LE were calculated by DICTRA, version 26 with TCFE5 and MOB2 databases. The initial ferrite thickness and austenite

thickness were 1×10^{-9} m and 6×10^{-6} m, respectively. The austenite grain was divided into 64 by geometric progression of 1.05. The ferrite/austenite interface was assumed to be linear.

The region containing an interface between ferrite and a variety of martensite and retained austenite (MA) in each material, which was ferrite/austenite interface at 973 K, was extracted and thinned by Focused Ion Beam (FIB) and Ar ion milling. The thinning process by FIB was performed by Hitachi FB2100. The acceleration voltage was 40 kV at the beginning and then decreased to 20 kV for the fine fabrication. Low voltage Ar ion milling was conducted to remove the surface damage that was caused during the FIB process. The acceleration voltage was 1 kV at the beginning and gradually decreased to 300 V.

The ferrite/MA interfaces were observed by aberration corrected STEM. Additionally, Mn concentration profiles near the ferrite/MA interfaces were measured by STEM-EELS. The STEM observation was performed by FEI Titan^3 80-300 at the acceleration voltage of 300 kV. To minimize the influence of the interface inclination on the measurement results of the Mn profile near the interfaces, the tilt series measurement technique was adopted [20]. The Mn concentration profiles were measured from two interfaces on respective specimens. The profiles which have higher concentration at the interface were chosen to be nearest to the true profiles.

3. RESULTS

Figure 1 shows an isothermal section of Fe-C-Mn ternary phase diagram with PLE, NPLE and PE region at 973 K. The open circle shows the matrix constitution of this specimen. It is below the NPLE limit. As a result, ferrite growth could follow NPLE or PE kinetics. The interfacial tie line in the figure shows that the equilibrium Mn concentrations in ferrite and austenite of NPLE mode is 2.0 and 6.2 mass %, respectively.

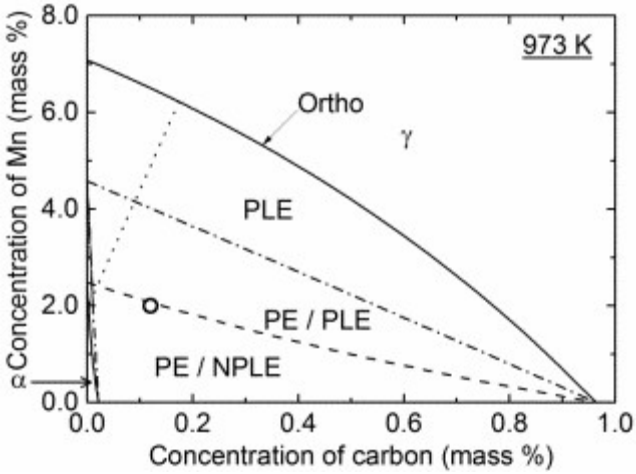

Fig. 1 Isothermal section of Fe-C-Mn ternary phase diagram at 973 K. Open circles, solid lines, alternating long and short dashed line, dashed line, and dotted line shows initial content, equilibrium boundary, PE boundaries, NPLE/PLE boundary, and tie-line of NPLE, respectively.

Figure 2 shows time dependence of the thickness of ferrite grains. In the optical microscope observation, the ferrite grains were primarily spherical in shape, which suggested that they were allotoriomorphic ferrite grains. The mean diameter of austenite grains was about 170 μm. The thickness of ferrite grains increased with the holding time and saturated after 3,000 s. It should be noted that the ferrite grains grew at a rate faster than that calculated under LE and slower than the one calculated under PE conditions.

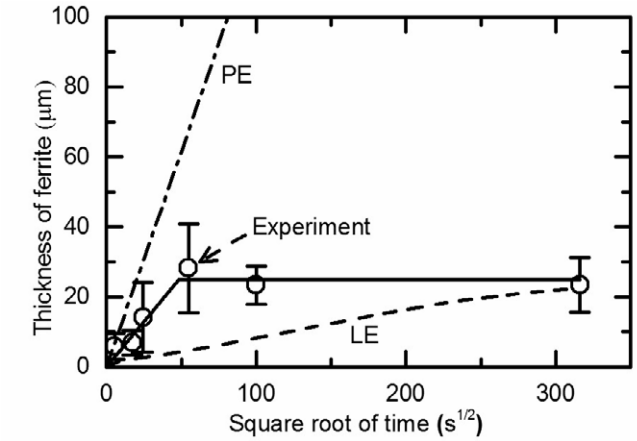

Fig. 2-Time dependence of the thickness of ferrite grain at 973 K. Open circles with error bars show thickness of ferrite obtained by optical microscope observation. Error bars show standard deviations. Alternate long and short dash line and dashed line show width of ferrite from austenite grain boundaries obtained by DICTRA calculation on PE and LE modes, respectively.

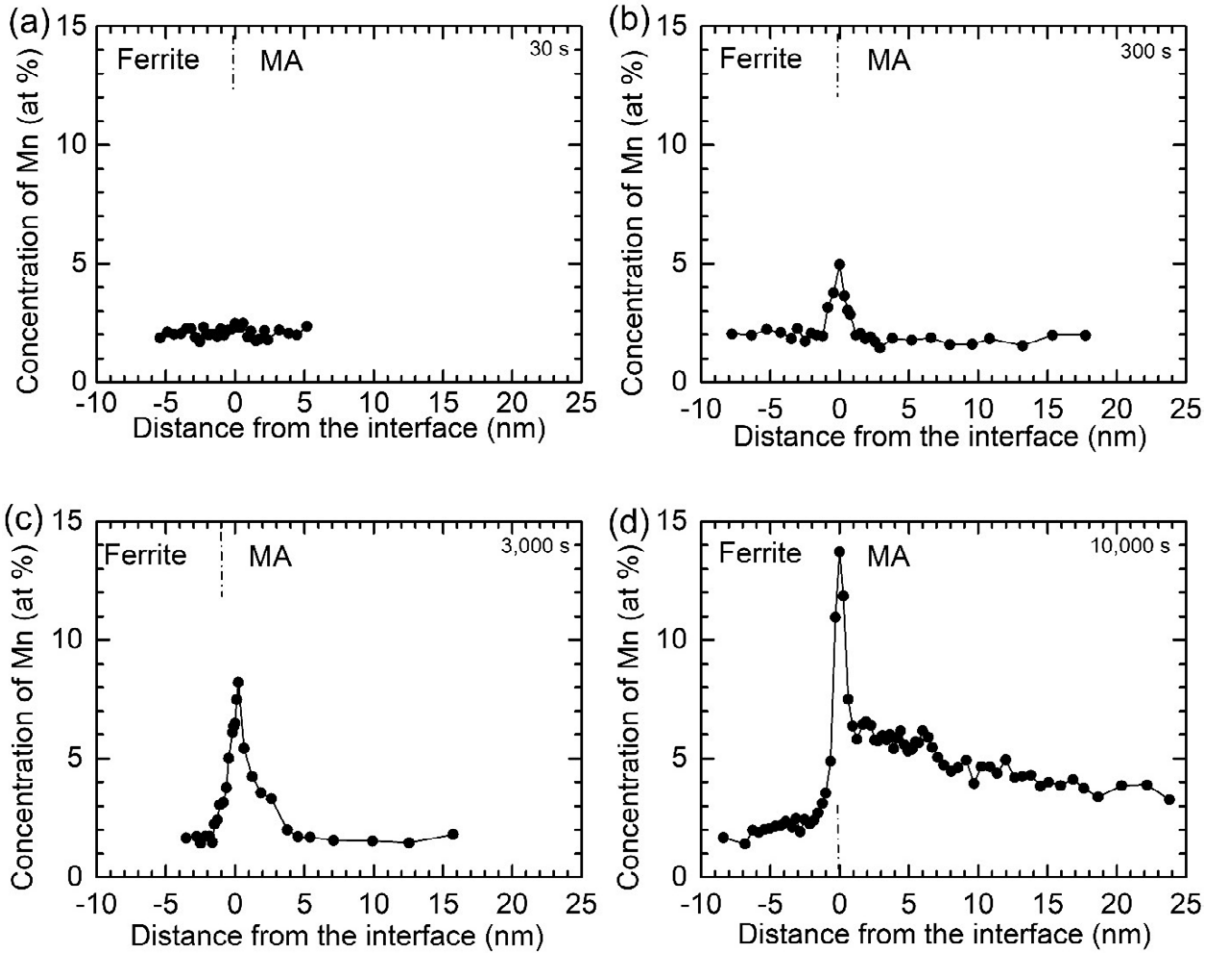

Fig. 3 Mn concentration profiles across the ferrite/MA interface of alloy Fe-0.12 mass % -2.0 mass % Mn after isothermal transformation at 973K measured by EELS. The incident electron beam diameter was about 0.2 nm. The maximum distance of specimen drift during the measurements per point was 0.3 nm perpendicular to the ferrite/MA interface. The specimen thicknesses in the analysis regions were 30, 25, 40 and 30 nm for holding times of 30, 300, 3,000, and 10,000 s, respectively.

Figure 3 shows the Mn concentration profiles for each of the holding times as measured by EELS. No specific feature of Mn distribution was recognized for the specimen after a holding time of 30 s. The Mn concentrations in ferrite and MA were equivalent. Enrichment of Mn at the interface was not

recognized (Fig.3 (a)). For a holding time of 300 s, the Mn concentration at the interface was higher than that of the matrix although there was still no difference between the concentrations within the ferrite and MA, respectively (Fig.3 (b)). When the holding time was increased, the concentration at the interface increased. The measured values of concentrations were 5, 8 and 14 at% for 300, 3,000, and 10,000 s, respectively. In the meantime, the Mn concentration in MA closed to the interface increased with a holding time exceeding 3,000 s (Fig.3 (c),(d)). The concentration decreased with the distance from the interface. The concentration measured at points far enough from the interface was about 2 at% for all conditions, which was consistent with the Mn content of the alloy. The width of the Mn enriched region in MA phase was about 5 nm at 3,000 s and 40 nm at 10,000 s.

4. DISCUSSION

4. 1. Measurement accuracy of the Mn concentration

In this study, Mn concentration was obtained by the following procedures. First the integral intensities of the Mn-L edge and Fe-L edge were extracted by subtracting the background components from an EELS spectrum. After that Mn concentration was estimated by the ratio of the intensities and the cross sections of the edges. The cross sections were estimated by the Hartree-Fock approximation in the current study. The measurement error of the concentration mainly comes from the statistical error of the spectrum, background model and the cross sections.

Since the intensities of Mn-L edges were about 70,000 counts, the statistical error was considered to be small, which was estimated to be about 0.004 by a simple estimation, $1/N^{0.5}$, where N is the signal count. For 2.0 at%, which is the Mn content of the material, it is equivalent to 0.01 at%.

In general, determination of the background components for EELS spectra is difficult [23]. This problem is remarkably the case for light elements, of which signals appear in a relatively low energy region, the result of analysis is very sensitive to the background subtraction process because the spectrum shape is very steep in a low energy region. For Mn-L edge and Fe-L edge, the background subtraction process is not so sensitive because the background shape is almost flat in the relevant energy region (Mn-L edge: 640 eV, Fe-L edge: 708 eV). However, when the signals of Mn-L edge were small, i.e. several at%, the background subtraction process can be a main cause of the error for the elemental quantification.

Although it is difficult to discriminate between those factors, the measurement errors in the current experiments are estimated below. The Mn concentrations of the matrices, that is, the concentrations at the points far enough from the interfaces, should be around the Mn content of the alloy, 2.0 at%. Mean concentrations measured in the matrix regions and the standard deviations in each specimen are summarized in Table 1. The difference of the concentration between specimens is considered to be due to the non-uniformity of the Mn distribution in the materials. The Mn concentration fluctuates over a range of tens of micrometers, which is called micro segregation. The average value of the matrix concentrations for 4 specimens was 1.98 at%, which was almost identical to the alloy content, 2.0 at%. Therefore, the accuracy of the quantification was considered to be very high. Moreover, the deviation of the matrix concentration in each specimen was less than 0.3 at%. Thus, the precision of the current analysis was estimated under 0.3 at %.

Table 1 Mn concentrations measured in the matrix regions and the standard deviations in the specimens held for 30, 300, 3,000, and 10,000 s at 973K.

	30 s	300 s	3000 s	10000 s	average
Mean concentration (at %)	2.1	1.9	1.7	2.2	1.98
Standard deviation (at %)	0.2	0.2	0.3	0.2	-

4. 2. Estimation of the true concentration profile

Although the incident beam diameter was quite small due to the advantage of aberration corrected STEM, which was as small as the lattice spacing of Fe, the spatial resolution of STEM-EELS analysis should be degraded by several factors (such as; the beam scattering in the specimen, the specimen drift during the measurement [20 24-26], convergence angle of the beam, and tilt angle of the interface from the direction of the beam). As a result, concentration profiles obtained by the measurement can be largely different from the true profiles. Thus, it is necessary to estimate the true profile from the obtained profiles for the detailed discussion of the phase transformation mechanism of allotriomorphic ferrite.

In order to estimate the true profiles, c_{Mn}^{γ}, $c_{Mn}^{\varphi/\gamma}$ and W were parameters for making the model profiles. In Figure 4, these parameters are described. First, model profiles were prepared using the parameters. Second, the expected profile, used to compare with the profile of the experimental result, was made by convolution between the model profile which has an inclination angle between the interface and the direction of the incident electron beam, and the electron beam intensity distribution, which is considered the broadening factors mentioned above. Third, the expected profile was compared with the profile of the experimental result. If the expected profile was consistent with the profile of the experimental result, it could be considered that the model profile was the true profile.

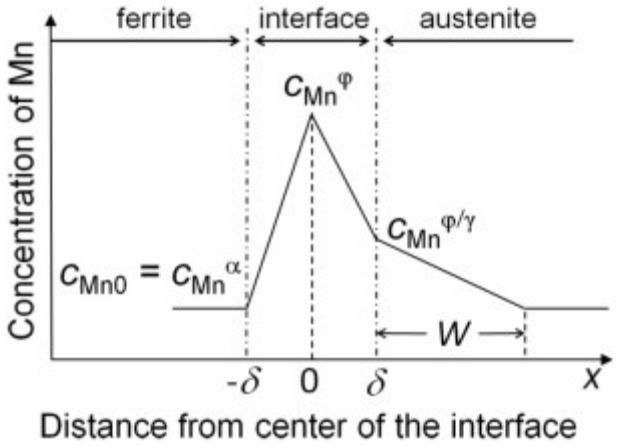

Fig. 4 Schematic profile of the Mn concentration near the interface. c_{Mn0} shows initial average concentration of Mn. In Fig. 4, the Mn concentration of ferrite region is close to c_{Mn0}. c_{Mn}^{φ} shows the Mn concentration at the center of the interface. $c_{Mn}^{\varphi/\gamma}$ shows the Mn concentration at the point of contact between the interface and the austenite. The width of the enrichment region in austenite is higher than c_{Mn0} as shown by W.

The calculated profiles obtained by the convolution are shown in Fig.5. In this simulation, the inclination of the interface plane to the electron beam was also considered. The inclination angles were determined to fit the calculated profiles with the measured ones. Each inclination angle suitable for a measured profile was determined among angles of 0.5 degrees intervals. For the specimen of 30 s, the measured profile was able to be explained by the profile with neither partitioning nor segregation (Fig. 5 (a)). The concentration was uniform for the entire area, which was 2.1 at %. For the specimen at 300 s, the experimental profile can be reproduced by considering the profile with the interfacial segregation, of which the concentration at the interface was 8.6 at%, and a 2-degree inclination of the interface plane (Fig. 5 (b)). For the specimens at 3,000 and 10,000 s, the experimental profiles can be assumed by the profiles with both partitioning and segregation under the condition of a 1.5-degree inclination and a zero-degree of the interface plane, respectively. The concentrations c_{Mn}^{φ} were estimated to be 13 at% and 20 at%, $c_{Mn}^{\varphi/\gamma}$ were 5.5 at% and 6.3 at%, the partitioning widths W were 4 nm and 40 nm for 3,000s and 10,000 s, respectively (Fig. 5 (c), (d)). c_{Mn0} of each holding time was used each mean concentration measured in the matrix region shown in Table 1.

4. 3. Mechanism of allotriomorphic ferrite formation at the first and second stage

Based on the above results, the behavior of Mn in the phase transformation will be discussed. In the specimen held at 973 K for 30 s, neither partitioning nor segregation occurred. Therefore, it is considered that allotriomorphic ferrite was formed by PE mode at the first stage.

At the second stage, allotriomorphic ferrite is considered to be formed by PE mode with interfacial segregation. The reasons are listed as follows. First, it is considered that partitioning of Mn from ferrite to austenite hardly occurred at 300 s. As shown in Fig. 5 (b), the measured profile can be interpreted with only segregation and no partitioning. The concentration at the interface was considered to be 8.6 at%, which was about 4.3 times higher than in the matrix. The meaning of the value will be discussed in the next section. Second, the growth rate of ferrite was faster than that expected for NPLE mode as shown in Fig. 2. If ferrite was formed by NPLE, the time dependence of the mean size of the ferrite grains in Fig. 2 would be expected to be on or below the LE line. Therefore, it is considered that the

mechanism of ferrite formation at 300 s is neither PLE nor NPLE. Meanwhile, the growth rate of the ferrite grain was slower than that expected under PE. Based on those facts, it is suggested that the mechanism of the ferrite formation at the second stage is PE with interfacial segregation. The growth rate was slower than that for PE because of the solute drag effect of Mn.

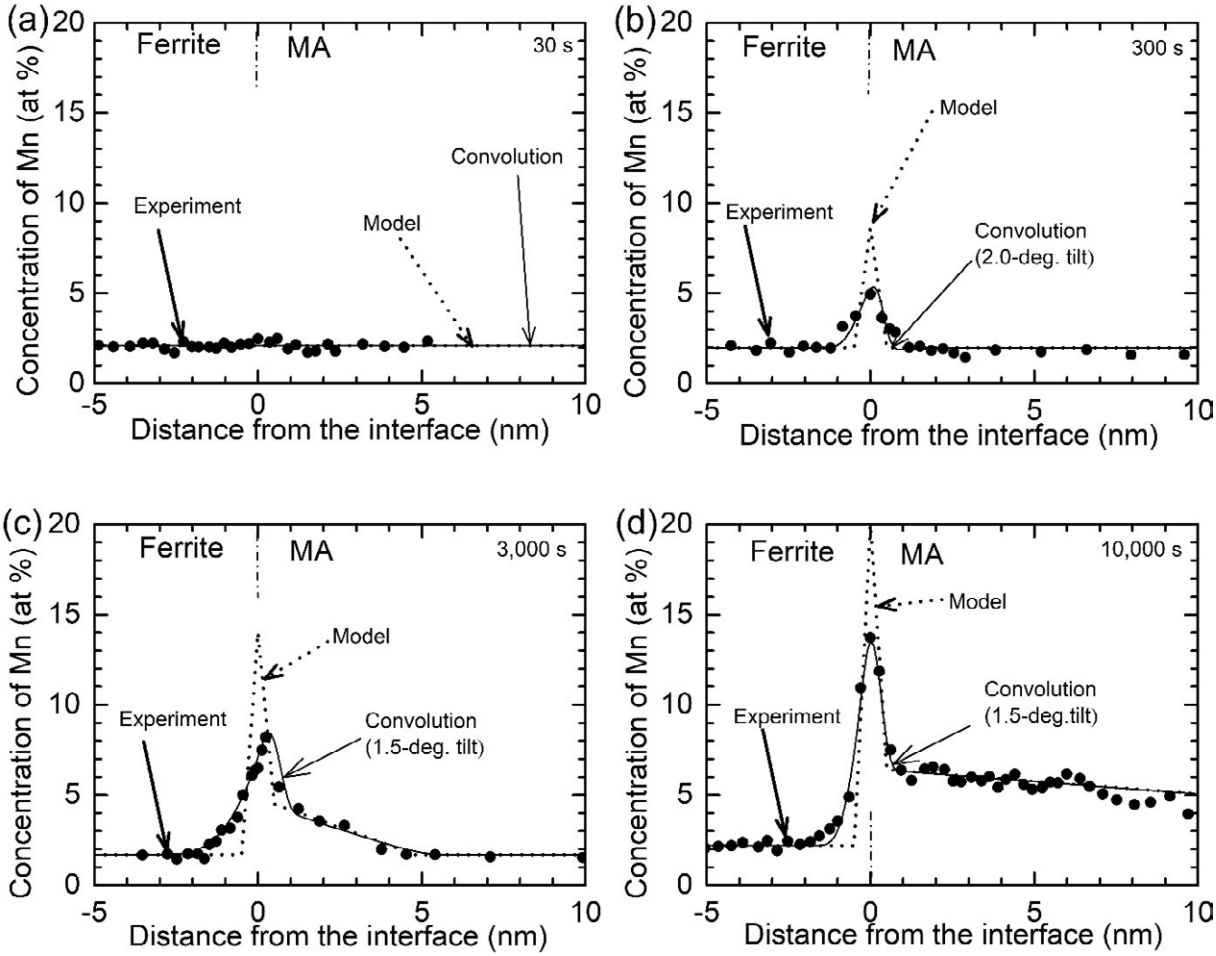

Fig. 5 Assumed and convoluted profiles with experimental results of Mn concentration using electron beam expansion.The calculated parameters included 0.3nm specimen drift per measurement position and tilt angle of the interface from the direction of the incident electron beam. Assumed Mn concentration profiles and profiles were obtained by convolution of the assumed profiles and the beam intensity distribution. The convolution profiles are close to experimental results. Assumed profiles corresponding with each convolution profile are estimated to be true profiles.

4. 4. Mechanism of allotriomorphic ferrite formation at the third and fourth stage

At the third stage, Mn partitioning occurred. The Mn concentration profiles in the specimens held at 973K for 3,000 s showed an apparent Mn enriched region on the MA side. The Mn concentration was higher than in the matrix within about 4 nm from the interface in the specimen of the holding time at 3,000 s. The concentration at the contact point between the interface and austenite at 3,000 s was smaller than 10,000 s. The concentration at the contact point at 10,000 s was estimated close to 6.3 at % which was the concentration of austenite in NPLE given by a Thermo Calc calculation. That means that Mn partitioning occurred on the phase transformation in the third stage but the stage had not achieved NPLE. In other words, the third stage is in the transition condition from PE to NPLE. However, in this stage, partitioning had already started. In the transition theory [6], partitioning should not occur before NPLE. Therefore, it is considered that partitioning occurred due to the moving rate of interface becoming slower than that of NPLE due to the solute drag effect.

The concentration in austenite adjacent to the interface, $c_{Mn}^{\varphi/\gamma}$, was 6.3 at% at 10,000 s. According to the calculation by Thermo Calc, $c_{Mn}^{\varphi/\gamma}$ is 6.3 at% for NPLE. However, the profile at 10,000 s shows the partitioning has already occurred. Therefore, this condition should not be in NPLE but PLE. In the

third stage, partitioning had already occurred. Therefore, it is considered that the transition from third to fourth stage proceeds without going through NPLE.

4. 5. Segregation to the ferrite/austenite interface

As shown in the previous sections, Mn segregation to ferrite/austenite interface was observed in all profiles after the second stage. As a result of that the ferrite growth rate was smaller than that of PE mode in the second stage, which was the so-called solute drag effect. In this section, the concentration profile of the solute drag is considered.

Quantitative treatment of the solute drag was first proposed by Cahn [27]. Purdy and Brechet [21] extended Cahn's theory to phase boundaries. After the Purdy-Brechet model, an asymmetrical wedge-shaped potential well for the interaction of solute *i* with the interface is considered. In Fig. 6, $2\Delta E$ is the chemical potential difference of *i* in austenite and ferrite, E_0 is the binding energy of *i* to the interface and 2δ is the width of the interface.

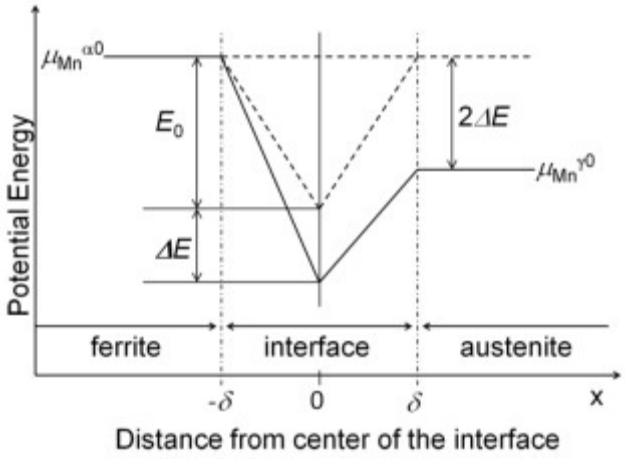

Fig. 6 Schematic showing the chemical potential profile near the interface. $\mu_{Mn}^{\alpha 0}$ and $\mu_{Mn}^{\gamma 0}$ show chemical potential of the ferrite and austenite phase, respectively. E_0 shows binding energy between Mn and the ferrite/austenite interface. δ shows the point halfway from the center of the interface.

The concentration profile ($c_i(x)$) of *i* at a moving interface with a quasi-steady-state velocity (v) is calculated by the flux equation [21].

$$\frac{\partial C}{\partial X}+\frac{C}{RT}\frac{\partial E}{\partial X}-V(C-1)=0 \qquad (3)$$

where C, X, and V are dimensionless parameters defined by $C=c_i/c_{io}$, $X=x/\delta$, $V=v\delta/D_b$, c_{io} is the bulk composition of *i* and D_b is the diffusivity across the interface. The concentration profile at the interface can be obtained by solving this equation.

The model profiles in Fig. 5 were able to fit to the profiles assumed by solute drag well. The parameter sets for simulating the four assumed profiles were found by using the solute drag calculation with fitting parameters, D_b= 2.8x10^{-18} m^2/s, E_0 =13 kJ/mol, and v(30 s)=2×10^{-7} m/s, v(300 s)=8×10^{-9} m/s, v(3000 s)=1×10^{-9} m/s, v(10000 s)=2×10^{-10} m/s. Each c_{Mn0} for the specimens held for 30, 300, 3,000, and 10,000 s were given the the mean concentration in Table 1. The calculated cell size was given 1×10^{-6} nm.

Figure 7 shows the time variation of the interfacial velocity comparison between the velocity estimated from optical microscope observation and that of the solute drag calculation. The velocity from the solute drag calculation was close to that of optical microscope observation.

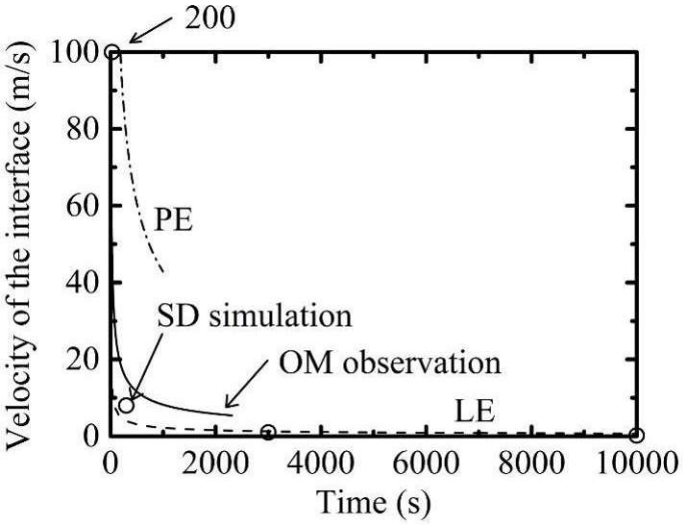

Fig. 7 Time variation of the interfacial velocity.

5. CONCLUSIONS

The present study investigated the formation behavior of allotriomorphic ferrite during isothermal annealing at 973 K in Fe-0.12C-2.0Mn (mass %) ternary alloy. The Mn concentration profiles near the transformation interfaces were investigated quantitatively using the aberration corrected STEM-EELS technique.

In the first and second stages, the size of the ferrite grains increased faster than the calculated result for the local-equilibrium condition and slower than that for the PE condition. In the third stage, the concentration profile couldn't be explained using the conventional transition theory. It is considered that that partitioning occurred due to the fact that the moving rate of interface became slower than that of NPLE caused by the solute drag effect. In the fourth stage, Mn concentration at the contact point at the austenite side was close to the concentration of NPLE calculated by Thermo Calc. However, partitioning had already occurred. Therefore, the fourth stage should be PLE. It is considered that the transition from third to fourth stage proceeds without going through NPLE.

The ferrite growth behavior estimated by optical microscope observation is close to the growth rate estimated by combining the STEM-EELS measurement and the SD theory.

REFERENCES

[1] D.E. Coates: Metall. Trans., 4 (1973), 2313-2325.
[2] A. Hultgren: Trans. ASM, 39 (1947), 915-1005.
[3] G. Purdy, J. Ågren, A. Borgenstam, Y. Bréchet, M. Enomoto, T. Furuhara, E. Gamsjager, M. Gouné, M. Hillert, C. Hutchinson, M. Militzer, and H. Zurob: Metall. Mater. Trans. A, 42A (2011), 3703-3718.
[4] C.R. Huchinson, A. Fuchsmann, and Y. Brechet: Metall. Mater. Trans. A, 35A (2004), 1211-1221.
[5] C. Capdevila, J. Cornide, K. Tanaka, K. Nakanishi, and E. Urones-Garrote: Metall. Mater. Trans. A, 42A (2011), 3719-3728.
[6] M. Hillert: Scripta Mater., 46 (2002), 447-453.
[7] G.R. Purdy, D.H. Weichert, and J.S. Kirkaldy: Trans. TMS-AIME, 230 (1964), 1025-1034.
[8] H.I. Aaronson, H.A. Domian, and G.M. Pound: AIME Met. Soc. Trans., 236 (1966), 768-781.
[9] J.B. Gilmour, G.R. Purdy, and J.S. Kirkaldy: Metall. Trans., 3 (1972), 3213-3222.
[10] K. Oi, C. Lux, and G.R. Purdy: Acta Mater., 48 (2000), 2147-2155.
[11] C.R. Huchinson, A. Fuchsmann, H.S. Zurob, and Y. Brechet: Scripta Mater., 50 (2004), 285-289.
[12] C.R. Huchinson, H.S. Zurob, and Y. Brechet: Metall. Mater. Trans. A, 37A (2006), 1711-1720.
[13] J. Odqvist, M. Hillert, and J. Ågren: Acta Mater., 50 (2002), 3211-3225.
[14] H.S. Zurob, C.R. Hutchinson, A. Béche, G.R. Purdy, and Y.J.M. Bréchet: Acta Mater., 56 (2008), 2203-2211.
[15] O. Thuillier, F. Danoix, M. Goune, and D. Blavette: Scripta Mater., 55 (2006), 1071-1074.
[16] M. Enomoto, C.L. White, and H.I. Aaronson: Metall. Trans. A, 19A (1988), 1807-1818.
[17] R. Wei, K. Kanno, and M. Enomoto: Metall. Mater. Trans. A, 42A (2011), 2189-2198.
[18] G.H. Zhang, Y.U. Heo, E.J. Song, and D.W. Suh: Met. Mater. Int., 19 (2013), 153-158.
[19] H. Guo, S.W. Yang, C.J. Shang, X.M. Wang, and X.L. He: J. Mater. Sci. Technol., 25 (2009), 383-388.
[20] G. Shigesato, T. Fujishiro, and T. Hara: Mater. Sci. Eng. A, 556 (2012), 358-365.
[21] G.R. Purdy and Y.J.M. Brechet: Acta Metall. Mater., 43 (1995), 3763-3774.

[22] F. Fazeli and M. Militzer: Metall. Mater. Trans. A, 36A (2005), 1395-1405.
[23] R.F. Egerton: Electron Energy-Loss Spectroscopy, Second ed. Plenum Press, New York, (1996).
[24] P. Doig and P.E.J. Flewitt: Micron and Microscopica Acta, 14 (1983), 225-231.
[25] I.A. Vatter and J.M. Titchmarsh: Ultramicroscopy, 28 (1989), 236-239.
[26] V. Keast and D.B. Williams: J. Microscopy, 199 (2000), 45-55.
[27] J.W. Cahn: Acta Metall., 10 (1962), 789-798.